Indication of single-crystal PuO_2 oxidation from O 1*s* x-ray absorption spectra

A. Modin, Y. Yun,* M.-T. Suzuki,† J. Vegelius, L. Werme, J. Nordgren, P. M. Oppeneer, and S. M. Butorin‡
Department of Physics and Astronomy, Uppsala University, P.O. Box 516, SE-751 20 Uppsala, Sweden
(Received 7 September 2010; revised manuscript received 19 November 2010; published 17 February 2011)

The electronic structure of single-crystal PuO_2 is studied using O 1*s* x-ray absorption (XA) and x-ray emission. Interpretation of the experimental data is supported by extensive first-principles calculations on the basis of the density functional theory + U approach. The measured XA spectra show a significant difference in intensity for the first two peaks between different spots or areas on the single crystal. Our theoretical simulations show that the first peak, at ∼531 eV, can be attributed to O 2*p*-Pu 5*f* hybridization, while the second peak, at ∼533.4 eV, is due to hybridization of O 2*p* with Pu *d* states. The reasons for the observed differences in the O 1*s* XA spectra are explored by calculating a number of defect structures $PuO_{2\pm x}$ as well as by simulating the existence of Pu(V) sites. Our results indicate the presence of oxidation states higher than Pu(IV) in some areas of the single crystal. The findings also suggest that plutonium oxide with a Pu fraction in an oxidation state higher than Pu(IV) consists of inequivalent Pu sites with $Pu^{(IV)}O_2$ and $Pu^{(V)}O_2$ rather than representing a system where the Pu oxidation state is constantly fluctuating between Pu(IV) and Pu(V).

DOI: 10.1103/PhysRevB.83.075113 PACS number(s): 71.28.+d, 78.70.En, 78.70.Dm, 71.20.−b

I. INTRODUCTION

Plutonium dioxide (PuO_2) has traditionally been considered to be the highest stable Pu oxide, but recent findings indicate that PuO_2 can react with water to form higher oxides up to $PuO_{2.27}$.[1,2] The existence of PuO_{2+x} is expected to have great consequences for the proposed underground disposal of nuclear waste since higher-oxidation-state plutonium species are much more water soluble than Pu(IV) species and, consequently, more mobile and can be transported from the waste repository to the biosphere.[3]

Since the discovery of PuO_{2+x} there has been an ongoing debate whether or not this higher oxide is thermodynamically stable. Theoretical studies cast doubts on the stability of PuO_{2+x}[4–6] and several experimental attempts to further oxidize PuO_2 using atomic oxygen or ozone have been unsuccessful.[7–9] In contrast, an x-ray photoelectron spectroscopy study[10] supplied evidence, especially in the O 1*s* region, of higher-valence Pu species in a sample formed by the reaction of high-fired PuO_2 with H_2O vapor at elevated temperatures.

While x-ray absorption (XA) spectroscopy probes unoccupied states and the local atomic environment of absorbing atoms, x-ray emission (XE) spectroscopy probes occupied states of the element in question. Thus, the techniques are complementary and provide a powerful tool for investigation of the local bonding environment and the electronic structure of studied atoms. Several XA studies have been reported on the Pu L_3 edge for plutonium oxides,[11–14] indicating an affinity to reaction with H_2O vapor, but there are no data available for the O 1*s* region.

Safe disposal of plutonium-containing waste requires an understanding of the possible behavior of the waste material when in contact with aqueous media. To achieve such an understanding, the electronic structure and the local bonding environment of plutonium, as well as its interaction with other substances that are present in the repository environment or in the biosphere, need to be studied. Here we present the first soft XE and XA spectroscopic data in the O 1*s* region for a single crystal of PuO_2. The interpretation of the experimental data is supported by extensive first-principles calculations within the framework of the local density approximation with supplemented intra-atomic Coulomb interaction U for the 5*f* electrons accounted for (LDA + U approach) as well as the generalized gradient approximation with an additional Coulomb U taken into account (GGA + U).

II. EXPERIMENTAL PROCEDURE

A. Samples

A single crystal of PuO_2 (with the Pu-239 isotope) was grown at the Laboratory of Applied Mineralogy and Radiogeochemistry of the V. G. Khlopin Radium Institute, St. Petersburg, Russia. Its synthesis was carried out by the flux method using the following flux composition: PuO_2 (5 wt%) and MoO_2 (95 wt%). A Pt crucible filled with flux and powder of PuO_2 was placed in a tube furnace[15] installed in a glove-box environment. Evaporated radioactive flux was accumulated inside a special silica-glass tube inside the furnace. Synthesis was carried out in air at 1100 °C for 72 h. To dissolve the rest of the flux, an ammonium-hydroxide aqueous solution (25%) was used. Finally, the chosen crystal, with a size of ∼2 mm^2, was rinsed in concentrated nitric acid and was then characterized by x-ray diffraction technique to confirm its phase composition and structure [unit cell parameter $a = 5.397(1)$ Å]. The aging time of the crystal before our measurements was 2 years.

The polycrystalline plutonium-242 dioxide sample used as a reference in the present measurements was fabricated by standard techniques used for the preparation of radionuclide counting plates. The counting plate was prepared from an aqueous solution of about 0.8 mM plutonium-242 in approximately 0.1 M HCl that was localized onto the surface of a high-purity platinum substrate (25.4-mm diameter, 0.05-mm thickness) by successive, partial micropipette aliquots into an area of about 2 mm^2. The isotopic composition of the plutonium solution was about 99.9% plutonium-242 and 0.1% in the suite of Pu isotopes (238–241), by mass.

B. X-ray absorption and emission measurements

Soft XA and XE measurements were performed at beamline I511-3,[16] MAX-lab, Lund, Sweden, which is equipped with a SX-700 plane-grating monochromator. The XA spectrum of polycrystalline PuO_2 that is used for reference purposes here was measured at beamline 7.0.1 (Ref. 17) at the Advanced Light Source, Berkeley, California, USA.

Tunable XE measurements were carried out using a high-resolution grazing incidence grating spectrometer with a movable multichannel detector.[18] The O K_α ($2p \rightarrow 1s$ transitions) spectra were recorded in first order of diffraction using a 5-m-radius spherical grating with 1200 lines/mm. The experimental resolution for the monochromator was set to 0.4 eV at 530 eV, while the spectrometer was set to a resolution slightly better than 0.6 eV at 530 eV. The O K_α emission energy scale was calibrated using a spin-orbit splitting value between the L_α and the L_β lines of a zinc metal. The uncertainty in the energy scale calibration is estimated as ± 0.5 eV. The O $1s$ XA spectra were recorded in the total fluorescence yield mode. Outgoing photons from the sample were detected at a 90° angle to the direction of the incident beam in the horizontal plane. Incident and outgoing angles for incoming and outgoing radiation were 45° to the sample surface. The incident photon beam was focused on a 20×30 μm ($v \times h$) spot on the sample.

An instrumental and experimental setup handling the requirements of a closed source of radioactivity was used for soft x-ray spectroscopic measurements of single-crystal PuO_2, while a standard open-source setup was used for the polycrystalline sample. The closed source of radioactivity setup consisted of a vacuum-sealed cell containing the sample, mounted on a tubing system to ensure compatibility with most standard manipulators. Soft x-rays penetrated a thin, diamondlike-carbon (0.3×1.5 mm in area and 100 nm thick) window separating the interior of the cell from the vacuum in the experimental chamber. The sample was positioned directly behind the window. The closed-source experimental system is explained in detail elsewhere.[19]

III. CALCULATIONS

Theoretical studies were performed using first-principles calculations based on the density-functional theory (DFT). The full-potential localized augmented plane wave (FP-LAPW) method including spin-orbit interaction[20] was applied, in two implementations, the KANSAI and WIEN2K[21] packages. For the DFT exchange-correlation functional we used the LDA as well as the GGA.[22] However, as we expect strong Coulomb interactions between relatively localized f electrons in PuO_2, it is essential to use the LDA + U or GGA + U method.[23] A few DFT + U studies of PuO_2 have been reported recently.[24–26] The LDA + U or GGA + U approach can capture strong on-site Coulomb correlations beyond those incorporated already in the LDA or GGA, through the addition of an extra intra-atomic Coulomb interaction U for f electrons. The value of the Hubbard U parameter applicable to PuO_2 is *a priori* unknown. Here, we follow the strategy that we first estimate the applicable value of U through LDA + U calculations for pure PuO_2 and comparison to measured XA and XE spectra. This comparison establishes an effective U_{eff} ($=U - J$) of about 5 eV for PuO_2. J is the exchange parameter, which can be safely estimated to range from 0 to 0.5 eV.[27] Previous GGA + U investigations[28] gave a value of $U_{\text{eff}} = 4$ eV for UO_2, consistent with our result. Subsequently, we perform GGA + U calculations for bulk PuO_2 and $PuO_{2\pm x}$ defect structures using the estimated value of U as well as considering variations in the U parameter, with the goal of determining whether Pu(V) is present in PuO_{2+x}. We further mention that both the fully localized limit and the around-mean-field form were adopted here to treat the so-called $+U$ double-counting term.[29,30] The used $+U$ implementations are designed to treat spin-orbit (Ref. 20) and Coulomb U effects on an equal footing.[31,32] In addition, we have performed so-called open-core approach calculations to probe the influence of completely localized f electrons.

IV. RESULTS AND DISCUSSION

Figure 1 displays the O K_α emission and O $1s$ XA spectra of the single-crystal PuO_2, measured with the closed-source setup, together with LDA + U ($U = 5$ eV, $J = 0.0$ eV) calculated spectra of nonmagnetic PuO_2, which were obtained by broadening the calculated density of O p states (also shown in Fig. 1). The broadening was consequently performed with a Lorentzian and a Gaussian function to account for the O $1s$ core-hole lifetime, instrument resolution, and other broadening effects, respectively. For the XE spectrum a linearly energy-dependent full width at half-maximum Lorentzian was used to account for the O $2p$ hole life in the valence band in the final state of the spectroscopic process. To compare experimental data with theoretical results, the recorded XA spectrum of the single-crystal PuO_2 was placed on the same energy scale as the recorded XE spectrum using the elastic peak in the emission spectra. Thereafter the recorded spectra were placed on a binding energy scale by aligning the top of the O $2p$ valence band in the recorded emission spectrum and in the calculations.

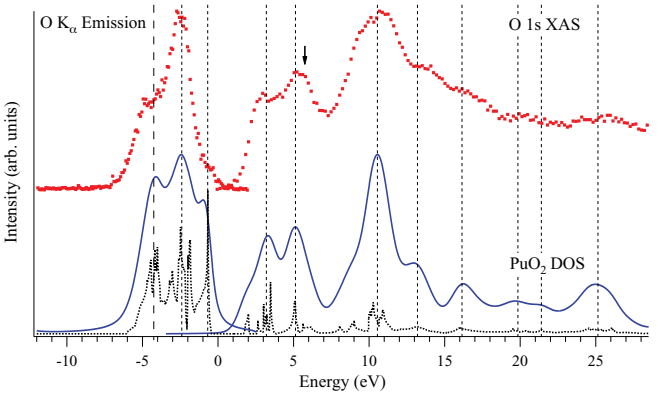

FIG. 1. (Color online) Experimentally recorded and LDA + U ($U = 5$ eV) calculated O K_α x-ray emission and O $1s$ x-ray absorption (XA) spectra of PuO_2. The incident photon energy of 533.6 eV used to record the x-ray emission spectrum corresponds to the excitation of O $1s$ electrons in the structure indicated by the arrow in the absorption spectrum. The calculated O p DOS is shown by the dotted curve.

The calculated emission spectrum resembles the experimentally recorded spectrum reasonably well, with the main structure at about −2.5 eV and a shoulder on the low-energy side at about −4.1 eV. The structure on the high-energy side of the main peak, at about −1 eV, is, however, overestimated in the calculations. The intensity of this structure grows with increasing value of the Coulomb interaction U used in the calculations, and the agreement with the measured XE spectra would be somewhat better for lower U values. The band gap, in contrast, is slightly underestimated in the calculations, and it would be even more underestimated upon using lower Coulomb interaction values, thus suggesting that $U_{\text{eff}} = 5$ eV is a reasonable choice for bulk PuO_2 in this LDA + U calculation.

The LDA + U calculated absorption spectrum is in close agreement with the experimental XA spectrum, showing spectral features around 3.2, 5.1, 10.6, 13.2, 16.2 19.9, 21.4, and 25.1 eV, indicated by dotted vertical lines in Fig. 1. We note, however, that some discrepancies also exist. There is a shoulder at 9.5 eV in the measured spectrum that has a much lower intensity in the calculation. At 4 eV there is more intensity in the measured XA spectrum, whereas in the calculation there is a deeper valley between the peaks at 3.2 and 5.1 eV. Also, the low-energy peak at 3.2 eV has a shoulder near 2 eV, which is less pronounced in the calculation. The structure at ∼3.2 eV is somewhat overestimated in the calculated spectrum, and as this overestimation is higher for lower values of the Hubbard parameter U, the use of $U_{\text{eff}} = 5$ eV is further justified.

The O 1s XA spectra of the single-crystal PuO_2 were measured for a number of randomly selected areas on the crystal. Figure 2 shows the XA spectra collected from three areas of the single crystal (SC) together with the XA spectrum for polycrystalline (PC) PuO_2. All spectra have similar main spectral features, with structures around 531, 533.4, 538.3, 539, 541.7, 544.5, 548.7, 554.1, and 566 eV. There is, however, a sizable difference in intensity for the first two peaks in

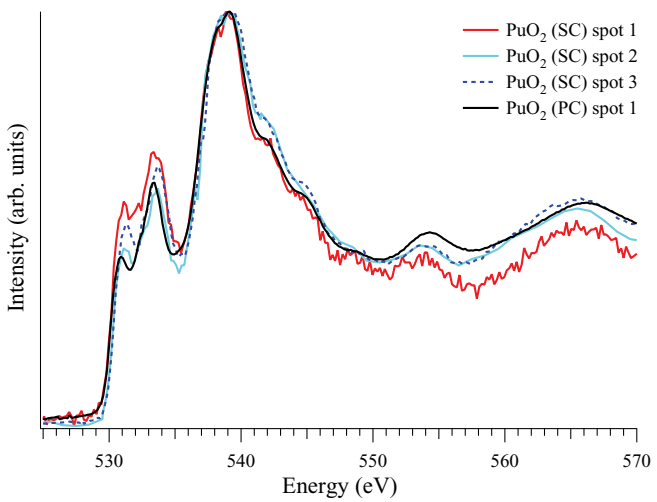

FIG. 2. (Color online) O 1s x-ray absorption spectra collected for three areas/spots on the PuO_2 single crystal (SC) together with O 1s absorption spectrum of polycrystalline (PC) plutonium dioxide. Spectra are normalized to the maximum and displayed on the incident photon energy scale.

different areas of the single crystal and the polycrystalline sample. It is clear that the structure at ∼531 eV has the lowest intensity for the polycrystalline sample, while all the measured areas/spots of the single crystal show a higher intensity for this spectral structure. Nevertheless, for some areas/spots the spectral intensity at ∼531 eV is as low as that of the polycrystalline sample. Our GGA + U results, discussed below, show that this peak can be attributed to O 2p-Pu 5f hybridization, while the peak at ∼533.4 eV largely arises from oxygen states hybridized with Pu d states.

The observed differences in the O 1s XA spectra from different spots cannot be attributed to the sample surface contamination. The x-ray penetration depth for the corresponding energies is estimated to be ∼500 Å, so the spectra measured in the fluorescence-yield mode are dominated by the contribution from the bulk of the sample. Note that spot 1 was closer to the end of the x-ray-transparent window, which resulted in poorer spectral statistics due to partial shadowing of outgoing photons from the sample.

Previous Pu 4d XA and Pu 5d resonant inelastic x-ray scattering measurements indicated the presence of a fraction of Pu in an oxidation state higher than Pu(IV) for the reference polycrystalline sample.[33] It is reasonable to expect that the lower Pu 5f occupancy (i.e., $5f^3$) for the higher oxidation state of Pu will influence O 2p-Pu 5f bonding and thus affect the spectral structure at ∼531 eV. The assumption here is that the O 1s XA spectrum in Fig. 2 with the highest intensity at ∼531 eV represents stoichiometric PuO_2, while spectra with the 531-eV-feature intensity close to that of the polycrystalline reference sample belong to some defect structures in corresponding areas/spots on the PuO_2 single crystal.

To understand the observed spectral changes in the low-excitation-energy region, a number of different defect structures $PuO_{2\pm x}$ were stimulated using the GGA + U method. For the sake of consistency, we first computed the XA spectrum of bulk stoichiometric PuO_2 for several different values of the Hubbard parameter U and exchange $J = 0.5$ eV. The XA spectra computed for different U values are compared to the experimentally recorded XA spectrum of the single-crystal PuO_2 sample in the upper panel in Fig. 3. Figure 3 shows, first, that the GGA + U and LDA + U approaches provide practically identical spectra and, second, that the best agreement, in terms of the position of the first low-energy peak and intensity ratio of the two first structures, between calculations and experiment is obtained using $U = 5$ eV. As the next step, we look into the bonding between O 2p and Pu 4f states in the low-energy part of the absorption spectrum, to understand changes caused by oxygen nonstoichiometry. To this end, we performed calculations for the following defect structures: Pu_8O_{15}, Pu_7O_{16}, Pu_4O_9, Pu_8O_{17}, and an Pu_8O_{17} Willis cluster,[34] using $U = 5$ eV for the Coulomb parameter.

Apart from substoichiometric Pu_8O_{15}, which was studied for comparison, the defect structures contain an excess of oxygen. Note that two different kinds of Pu_8O_{17} structures were calculated to investigate oxygen stoichiometry exceeding that of PuO_2. When an additional oxygen atom is incorporated in the cubic fluorite structure, a so-called cubo-octahedral interstitial site is known to be energetically the most stable site

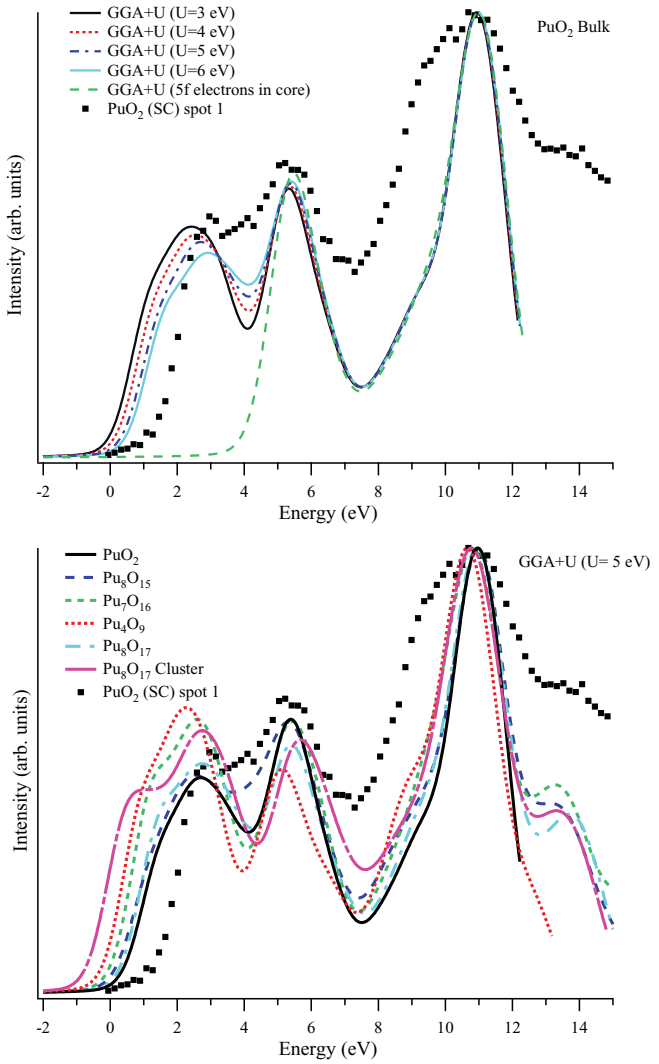

FIG. 3. (Color online) Top: GGA + U calculated x-ray absorption spectra for different values of U together with one experimentally recorded XA spectrum of the single-crystal sample. Bottom: All calculated absorption spectra for defect structures are shown together with that of stoichiometric PuO_2 and its experimental XA spectrum.

for the excess oxygen.[35] Willis (Ref. 34) proposed that fluorite compounds containing an excess anion consist of a defect cluster, a so-called 2:1:2 Willis cluster, in which the excess oxygen is located at an interstitial site along the (110) direction and the two nearest oxygen atoms are displaced toward the (111) directions, resulting in the creation of two interstitial oxygens and two oxygen vacancies. In this study, Pu_8O_{17} indicates that the additional oxygen atom is incorporated at a cubo-octahedral interstitial site, whereas the notation Pu_8O_{17} cluster denotes a defect structure of PuO_2 containing a 2:1:2 Willis cluster.

An important finding from the top graph in Fig. 3 is that in the open-core calculations (dashed curve), where all 5f valence electrons are forced to the core and therefore cannot hybridize with the O 2p states, the first low-energy structure, at about 2 eV, in the calculated absorption spectrum is missing. Thus, the presence of this low-energy structure in the experimentally recorded XA spectrum (shown by markers) can be attributed to O 2p-Pu 5f hybridization. The results of the open-core calculations also indicate that the second peak in Fig. 3, at about 5.5 eV, mainly originates from mixing between O 2p states with Pu d states.

The GGA + U calculated XA spectra were broadened in the same manner as for the LDA + U calculations, then put on the same energy scale as the measured XA spectrum by aligning the top of the valence O 2p band between experiment and theory. The results of GGA + U calculations for different defect structures together with those for stoichiometric PuO_2 and the experimentally recorded XA spectrum for the single crystal are shown in the bottom panel in Fig. 3.

All calculated absorption spectra show a higher intensity of the O 2p-Pu 5f hybridization peak at about 2 eV for the defect structures $PuO_{2\pm x}$ compared to that of stoichiometric PuO_2, while all but Pu_8O_{15} reveal a lower intensity in the second peak at ~5.5 eV. In particular, the absorption spectra for Pu_8O_{17} and Pu_4O_9 ($PuO_{2.125}$ and $PuO_{2.25}$, respectively) exhibit a growing O 2p-Pu 5f hybridization structure with increasing oxygen content, yielding the largest increase for Pu_4O_9. This results in an increased spectral intensity below 2 eV for the simulated defect structures. For measured XA spectra the behavior is opposite, however, with a higher intensity in the first peak, at ~2 eV, for the single-crystal PuO_2 area/spot, which is believed to have only Pu(IV), in comparison with the polycrystalline sample with the detected presence of the Pu fraction in an oxidation state higher than IV. Hence, the higher oxidation state of Pu, leading to a lowering of the intensity of the first peak, is not reflected in the simulated superstoichiometric oxygen defect structures.

A possible explanation for this contradictory behavior is that the redistribution of charges due to the self-consistent nature of the GGA + U method causes all Pu sites in the calculation to be equal, while in reality there might be inequivalent Pu sites with Pu(IV) and Pu(V), respectively.

To simulate Pu(V) sites, GGA + U calculations for charged PuO_2^{1+} and PuO_2^{2+} were performed using the 5-eV value for the Hubbard parameter U. In addition, a calculation for PuO_2 with plutonium enforced to be Pu(V) was carried out, where the initial density matrix was altered manually to contain only three Pu 5f valence electrons and the relaxation from this energetically unfavorable configuration was prevented by using a strong Coulomb interaction ($U = 22$ eV). The calculated total, partial O 2p, and partial Pu 5f densities of states (DOSs) of neutral, charged, and defected PuO_2 are displayed in Fig. 4.

The computed DOS illustrates that our nonmagnetic GGA + U calculations predict PuO_2 to be an insulator with a band gap of 1.7 eV. There is a significant amount of hybridization of the occupied Pu 5f states and O 2p states. Less O 2p-Pu 5f hybridization occurs for unoccupied states; the 5f's are hence narrower, leading to sharper peaks in the partial DOS. Upon removal of one or two electron charges, we observe from the self-consistent partial DOSs that PuO_2^{1+} and PuO_2^{2+} remain insulators, but with a reduced energy gap of 1 eV. The removal of an electron charge leads to an increase in the unoccupied Pu 5f and O 2p partial DOSs. Relevant to the O 1s XA measurements is, in particular, the appearance of more Pu 5f and O 2p DOSs just above the gap. The partial DOSs of

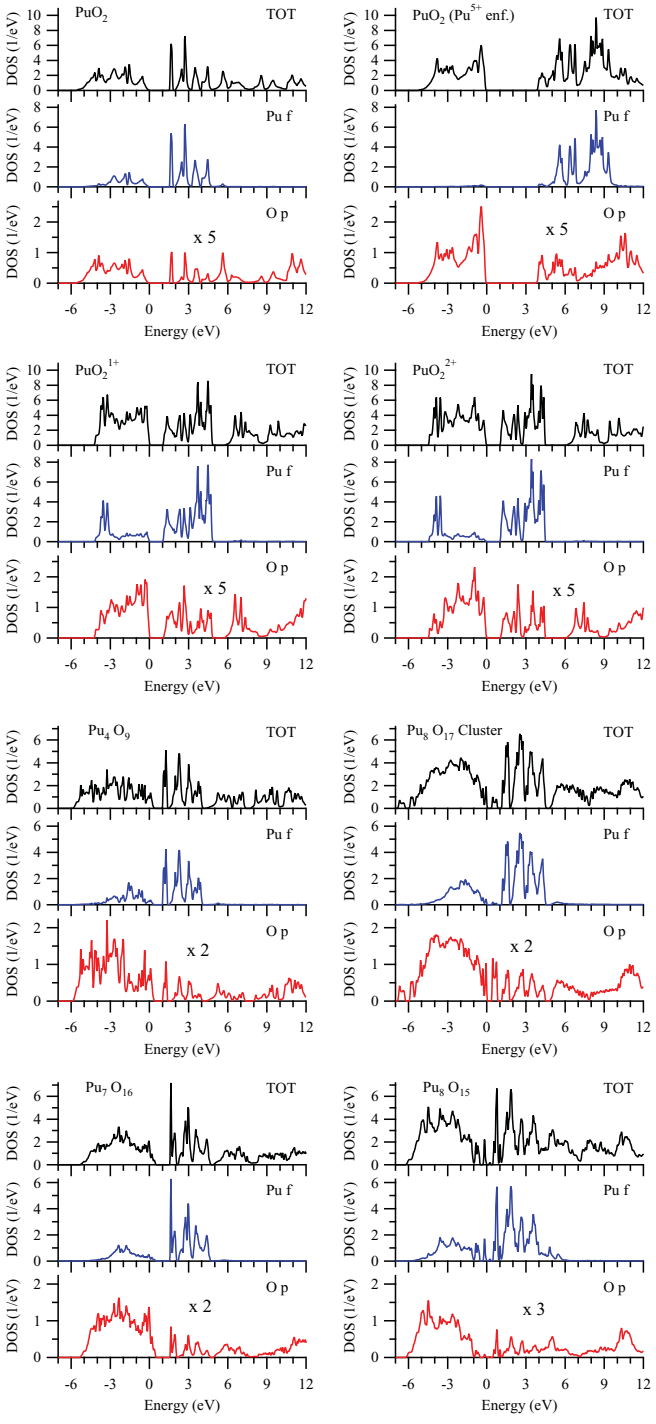

FIG. 4. (Color online) GGA + U calculated total (TOT; including Pu d), partial O $2p$, and partial Pu $5f$ density of states (DOS) for stoichiometric $Pu^{(IV)}O_2$, for two charged systems, PuO_2^{1+} and PuO_2^{2+}, for $Pu^{(V)}O_2$ with plutonium enforced to Pu(V) [enf.]. Computed total and partial DOSs of PuO_2 defect structures are also shown (bottom four panels). Unoccupied parts of O p DOSs were scaled up for clarity by factors indicated in the corresponding subpanels.

PuO_2 defect structures show that an oxygen surplus leads to loss of the insulating property for Pu_4O_9 and Pu_7O_{16}. A gap in the excitation spectrum still exists, but this gap is now placed in the unoccupied part of the DOS. Pu_8O_{17} with a 2:1:2 Willis cluster stays almost an insulator, with a gap that has become very small just above the Fermi level. The O $2p$ partial DOSs increase for oxygen surplus defect structures, as expected. The width of the $5f$ partial DOS increases substantially for the Pu_8O_{17} cluster and substoichiometric Pu_2O_{15}, indicating stronger Pu $5f$-O $2p$ hybridization. We note that also for the defect structures Pu $5f$ and O $2p$, a partial DOS appears in the energy interval where the gap in PuO_2 was located, something that is not supported by the XA experiments.

TABLE I. Calculated Pu $5f$ and O $2p$ occupancy for stoichiometric plutonium dioxide, PuO_2^{1+}, PuO_2^{2+}, and $Pu^{(V)}O_2$.

Occupancy	$Pu^{(IV)}O_2$	PuO_2^{1+}	PuO_2^{2+}	$Pu^{(V)}O_2$
Pu $5f$	4.30	3.77	3.60	3.18
O $2p$	4.47	4.34	4.11	4.53

The computed Pu $5f$ and O $2p$ occupancies of neutral $Pu^{(IV)}O_2$, $Pu^{(V)}O_2$, and charged PuO_2 are summarized in Table I. The information in Table I implies that removal of one or two electron charges from $Pu^{(IV)}O_2$ is not sufficient to enforce a valency reduction to $Pu^{(V)}$. Rather, as the partial DOSs in Fig. 4 show, the electron charge is removed from both O and Pu orbitals, with the Pu $5f$ occupation being depleted more than the O $2p$ occupation. Yet, as can be recognized from Table I, a Pu(V), that is, $5f^3$, occupation cannot be reached through electron removal. To this end, we have to enforce a $5f^3$ configuration through a large Coulomb U. The partial DOS in Fig. 4 shows that, in comparison to $Pu^{(IV)}O_2$, now DOS has been removed at energies above the gap. The consequence of this reduction of states is that the peak at 2–3 eV in the O $1s$ XA spectrum of $Pu^{(IV)}O_2$ will become strongly suppressed for $Pu^{(V)}O_2$, as discussed below.

The partial O $2p$ DOSs obtained in Pu(V) simulations were broadened and put on the same energy scale as the measured spectra in the same manner as for the LDA + U and GGA + U calculations discussed above. The resulting calculated absorption spectra for PuO_2^{1+}, PuO_2^{2+}, and PuO_2 with plutonium enforced to be Pu(V) ($Pu^{(V)}O_2$) are shown in Fig. 5, together with that of stoichiometric PuO_2 ($Pu^{(IV)}O_2$) and one experimentally collected XA spectrum as a reference.

The calculated absorption spectra of PuO_2^{1+} and PuO_2^{2+} show a significant increase in intensity of the first structure, which in these systems is split up into two features at about 1.2 and 2.6 eV, respectively. The charging-induced DOS modification above the gap in Fig. 4 is responsible for the split peak developing in the related O $1s$ XAS. The splitting of the first structure can also be seen for the Pu_8O_{17} cluster calculation (see Fig. 3), but it is not present in the measured spectra. In contrast, the first structure is suppressed in the GGA + U calculated XA spectrum for $Pu^{(V)}O_2$, suggesting that a linear combination of the calculated spectra of stoichiometric PuO_2 and PuO_2 with plutonium enforced to Pu(V) will yield the same behavior as for the measured XA spectra, that is, a lower intensity in the first peak for the higher oxidation state for Pu.

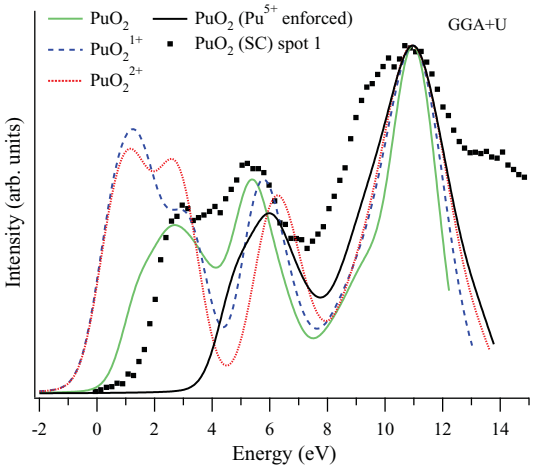

FIG. 5. (Color online) GGA + U calculated absorption spectra for the simulated Pu(V) systems PuO_2^{1+}, PuO_2^{2+} ($U = 5$ eV), and PuO_2 with plutonium enforced to be Pu(V) (using $U = 22$ eV to prevent relaxation), together with calculated absorption spectra for stoichiometric PuO_2 and one experimentally recorded XA spectrum for the PuO_2 single-crystal (SC) sample.

The linear combination is constructed by adding the right proportions of $Pu^{(IV)}O_2$ and $Pu^{(V)}O_2$, according to the equation

$$Pu^{(4+\alpha)}O_2 = \alpha Pu^{(V)}O_2 + (1-\alpha)Pu^{(IV)}O_2, \qquad (1)$$

where $0 \leqslant \alpha \leqslant 1$.

The results of linear combinations of $Pu^{(IV)}O_2$ and $Pu^{(V)}O_2$ for the α values of 0.25, 0.125, and 0.05 are shown, together with calculated stoichiometric PuO_2 and PuO_2 with plutonium enforced to Pu(V) and experimentally recorded XA spectra for single-crystal and polycrystalline plutonium dioxide, in Fig. 6.

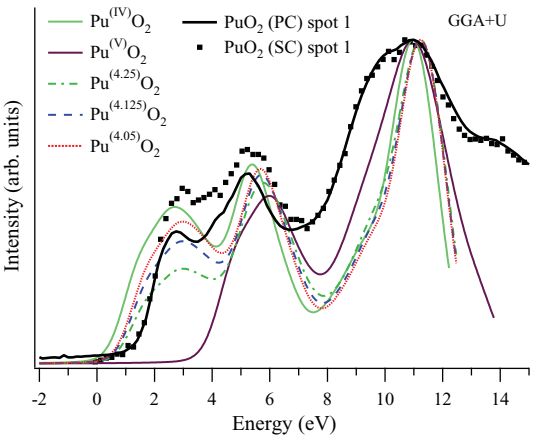

FIG. 6. (Color online) GGA + U calculated absorption spectra for stoichiometric PuO_2 and PuO_2 with plutonium enforced to Pu(V) together with linear combinations of the two calculations corresponding to $Pu^{(4.25)}O_2$, $Pu^{(4.125)}O_2$, and $Pu^{(4.05)}O_2$. Experimentally recorded XA spectra for single-crystal (SC) and polycrystalline (PC) plutonium dioxide are also shown for reference.

The linearly combined spectra clearly show a trend of decreasing intensity of the first low-energy peak with increasing fraction of Pu(V) species, which is in line with the interpretation of the experimental results. The calculated PuO_2 spectrum resembles the experimentally recorded spectrum for single-crystal Pu dioxide reasonably well, while the height of the first peak in the experimental XA spectrum of the polycrystalline sample is found to be between those for the linearly combined spectra of $Pu^{(4.125)}O_2$ and $Pu^{(4.05)}O_2$. This suggests the presence of an ∼8% fraction of Pu(V) in the polycrystalline sample, which is in line with previous Pu 4d XA and Pu 5d resonant inelastic x-ray scattering measurements for this sample.[33]

Figure 2 shows that XA spectra collected at spots 2 and 3 on the single-crystal PuO_2 show a similar trend of decreasing intensity of the first peak compared with spot 1, thus suggesting that those areas/spots of the single crystal have some fraction of plutonium in an oxidation state higher than Pu(IV).

V. CONCLUSION

We have performed an x-ray spectroscopic investigation of the electronic structure of an aged single crystal of PuO_2, followed by extensive theoretical analysis of experimental data obtained with advanced theoretical methods for strongly correlated systems. The measured O K_α XE and O 1s absorption spectra can be well explained by LDA + U and GGA + U calculations using a Coulomb U of about 5 eV. An analysis of the calculated spectra shows that the first peak in the XA spectrum is sensitively due to O 2p states hybridized with Pu 5f states. The reduction of this peak can be positively correlated with the appearance of nonstoichiometric PuO_{2+x} structures. Our combined experimental-computational investigations indicate the presence of some fraction of plutonium in an oxidation state higher than Pu(IV). The amount of this fraction is estimated to be as high as ∼8% for some local areas of the studied sample. Our results also suggest that plutonium oxide with a Pu fraction in an oxidation state higher than Pu(IV) consists of inequivalent Pu sites with $Pu^{(IV)}O_2$ and $Pu^{(V)}O_2$ rather than representing a system where the Pu oxidation state is constantly fluctuating between Pu(IV) and Pu(V). Our study emphasizes that possible oxidation of PuO_2 cannot be ruled out and that further research on specific regions of the Pu-O phase diagram is necessary.

ACKNOWLEDGMENTS

Financial support for this work was provided by the Swedish Research Council (VR), Svensk Kärnbränslehantering AB (SKB), and the Göran Gustafssons Stiftelse. The personnel of beamline I511-3 at MAX-lab are gratefully acknowledged for their assistance during measurements. The authors would like to thank Jan Rusz for his assistance with GGA + U calculations. We also acknowledge computer time received from the Swedish National Infrastructure for Computing (SNIC).

*Present address: Laboratory of Reactor Physics and Systems Behaviour, Paul Scherrer Institut, CH-5232 Villigen PSI, Switzerland
†Present address: Center for Computational Science & e-Systems Japan Atomic Energy Agency, 6-9-3 Higashi-Ueno, Taito-ku, Tokyo 110-0015, Japan
‡Corresponding author: sergei.butorin@fysik.uu.se

[1] J. M. Haschke, T. H. Allen, and L. A. Morales, Science **287**, 285 (2000).
[2] J. M. Haschke and T. H. Allen, J. Alloys Compd. **336**, 124 (2002).
[3] C. Madic, Science **287**, 243 (2000).
[4] L. Petit, A. Svane, Z. Szotek, and W. M. Temmerman, Science **301**, 498 (2003).
[5] P. A. Korzhavyi, L. Vitos, D. A. Andersson, and B. Johansson, Nat. Mater. **3**, 225 (2004).
[6] D. A. Andersson, J. Lezama, B. P. Uberuaga, C. Deo, and S. D. Conradson, Phys. Rev. B **79**, 024110 (2009).
[7] C. Keller, in *Comprehensive Inorganic Chemistry*, edited by J. C. Bailar, H. J. Emeleus, R. Nyholm, and A. F. Trotman-Dickenson (Pergamon, Oxford, 1973), Vol. 5, pp. 219–276.
[8] L. R. Morss, in *The Chemistry of the Actinide Elements*, 2nd ed., edited by J. J. Katz, G. T. Seaborg, and L. R. Morss (Chapman and Hall, London, 1986), Vol. 2.
[9] T. Gouder, A. Seibert, L. Havela, and J. Rebizant, Surf. Sci. **601**, L77 (2007).
[10] J. D. Farr, R. K. Schulze, and M. P. Neu, J. Nucl. Mater. **328**, 124 (2004).
[11] S. Conradson *et al.*, Inorg. Chem. **43**, 116 (2004).
[12] S. Conradson *et al.*, J. Solid State Chem. **178**, 521 (2005).
[13] S. Conradson *et al.*, J. Am. Chem. Soc. **126**, 13443 (2004).
[14] P. Martin, J. Nucl. Mater. **320**, 138 (2003).
[15] A. A. Kitsay, V. M. Garbuzov, and B. E. Burakov, in *Scientific Basis for Nuclear Waste Management XXVII, Stockholm, Sweden, 2004, Materials Research Society Symposium Proceedings Series*, edited by V. M. Oversby and L. O. Werme (Mater. Res. Soc., Warrendale, PA, 2004), Vol. 807, pp. 237–242.
[16] R. Denecke, P. Vaterlein, M. Bassler, N. Wassdahl, S. Butorin, A. Nilsson, J.-E. Rubensson, J. Nordgren, N. Mårtensson, and R. Nyholm, J. Electron Spectrosc. Relat. Phenom. **101–103**, 971 (1999).
[17] T. Warwick, P. Heimann, D. Mossessian, W. McKinney, and H. Padmore, Rev. Sci. Instrum. **66**, 2037 (1995).
[18] J. Nordgren and R. Nyholm, Nucl. Instrum. Methods Phys. Res. Sect. A **246**, 242 (1986).
[19] A. Modin *et al.*, Rev. Sci. Instrum. **79**, 093103 (2008).
[20] J. Kuneš, P. Novák, M. Diviš, and P. M. Oppeneer, Phys. Rev. B **63**, 205111 (2001).
[21] P. Blaha, K. Schwarz, G. K. H. Madsen, D. Kvasnicka, and J. Luitz, *Wien2k, an Augmented Plane Wave + Local Orbitals Program for Calculating Crystal Properties* (Techn. Univ. Wien, Austria, 2001).
[22] J. P. Perdew, K. Burke, and M. Ernzerhof, Phys. Rev. Lett. **77**, 3865 (1996).
[23] V. I. Anisimov, J. Zaanen, and O. K. Andersen, Phys. Rev. B **44**, 943 (1991).
[24] G. Jomard, B. Amadon, F. Bottin, and M. Torrent, Phys. Rev. B **78**, 075125 (2008).
[25] B. Sun, P. Zhang, and X.-G. Zhao, J. Chem. Phys. **128**, 084705 (2008).
[26] I. D. Prodan, G. E. Scuseria, and R. L. Martin, Phys. Rev. B **76**, 033101 (2007).
[27] Note that in the applied $+U$ formulation, U_{eff} is the determining quantity, not U or J separately.
[28] S. L. Dudarev, D. Nguyen Manh, and A. P. Sutton, Philos. Mag. B **75**, 613 (1997).
[29] V. I. Anisimov, I. V. Solovyev, M. A. Korotin, M. T. Czyżyk, and G. A. Sawatzky, Phys. Rev. B **48**, 16929 (1993).
[30] M. T. Czyżyk and G. A. Sawatzky, Phys. Rev. B **49**, 14211 (1994).
[31] A. B. Shick, A. I. Liechtenstein, and W. E. Pickett, Phys. Rev. B **60**, 10763 (1999).
[32] M.-T. Suzuki and H. Harima, J. Phys. Soc. Jpn. **79**, 024705 (2010).
[33] S. M. Butorin, K. O. Kvashnina, A. Modin, J.-H. Guo, D. K. Shuh, L. Werme, and J. Nordgren, Tech. Rep., SKB TR-09-08 (2009).
[34] B. T. M. Willis, Nature (London) **197**, 755 (1963).
[35] J. P. Crocombette, F. Jollet, T. N. Le, and T. Petit, Phys. Rev. B **64**, 104107 (2001).